Am J Physiol Cell Physiol 325: C314–C323, 2023.
First published June 19, 2023; doi:10.1152/ajpcell.00106.2023

american physiological society

AMERICAN JOURNAL OF PHYSIOLOGY
CELL PHYSIOLOGY

RESEARCH ARTICLE

Extracellular matrix composition alters endothelial force transmission

Vignesh Aravind Subramanian Balachandar[1,2] and Robert L. Steward, Jr.[1,3]

[1]*Department of Mechanical and Aerospace Engineering, College of Engineering and Computer Science, University of Central Florida, Orlando, Florida, United States;* [2]*Department of Cell Biology, University of Virginia, Charlottesville, Virginia, United States; and* [3]*Burnett School of Biomedical Sciences, College of Medicine, University of Central Florida, Orlando, Florida, United States*

Abstract

Extracellular matrix (ECM) composition is important in a host of pathophysiological processes such as angiogenesis, atherosclerosis, and diabetes, and during each of these processes ECM composition has been reported to change over time. However, the impact ECM composition has on the ability of endothelium to respond mechanically is currently unknown. Therefore, in this study, we seeded human umbilical vein endothelial cells (HUVECs) onto soft hydrogels coated with an ECM concentration of 0.1 mg/mL at the following collagen I (Col-I) and fibronectin (FN) ratios: 100% Col-I, 75% Col-I-25% FN, 50% Col-I-50% FN, 25% Col-I-75% FN, and 100% FN. We subsequently measured tractions, intercellular stresses, strain energy, cell morphology, and cell velocity. Our results revealed that tractions and strain energy are maximal at 50% Col-I-50% FN and minimal at 100% Col-I and 100% FN. Intercellular stress response was maximal on 50% Col-I-50% FN and minimal on 25% Col-I-75% FN. Cell area and cell circularity displayed a divergent relationship for different Col-I and FN ratios. We believe that these results will be of great importance to the cardiovascular field, biomedical field, and cell mechanics.

NEW & NOTEWORTHY The endothelium constitutes the innermost layer of all blood vessels and plays an important role in vascular physiology and pathology. During certain vascular diseases, the extracellular matrix has been suggested to transition from a collagen-rich matrix to a fibronectin-rich matrix. In this study, we demonstrate the impact various collagen and fibronectin ratios have on endothelial biomechanical and morphological response.

extracellular matrix; fibronectin; intercellular stresses; traction force microscopy; type 1 collagen

INTRODUCTION

The extracellular matrix (ECM) has recently been appreciated to serve as a biochemical signaling reservoir in addition to serving as the underlying scaffolding that anchors cells to their surrounding environment (1–3). Within blood vessels, the ECM separates the tunica adventitia (outer layer), tunica media (middle layer), and tunica intima (inner layer), but it is the endothelial cells that make up the tunica intima layer a major regulator of vascular pathology and physiology (3). Under normal conditions, each blood vessel layer is separated by unique ECM proteins; type IV collagen, fibronectin (FN), and laminin are found between the adventitia and media layers, whereas collagen I (Col-I) and elastin are found between the intima and media layer, but ECM composition can and does change during various pathologies (4). During pancreatic cancer, altered Col-I, FN, proteoglycans, and hyaluronic acid have been observed and suggested to lead to desmoplasia (5). Furthermore, impaired wound healing is a trademark of diabetes and has also been linked to increased ECM stiffness and ECM degradation as seen in fibroblasts (6). In fact, during diabetes, collagen and elastin fiber production has been suggested to decrease, whereas tissue FN production increases, reflecting a change in native ECM composition (6). Also, aging has been linked to a two- to threefold increase in intima-media thickness due to ECM remodeling from 20 to 90 yr in humans (7). There was a reduction in relative elastin, but twofold increase in collagen levels in rat aorta on comparison between 6 and 30 mo of age (8). Keeley et al. (9) also showed increase in collagen and elastin synthesis due to increased blood pressure during hypertension. Meanwhile, fibronectin deposition is shown to occur through increased vascular permeability due to injury or wound, promoting inflammation and atherosclerosis (10, 11). The impacts mentioned earlier reflect the biochemical changes that occur to the ECM, but the pathological and physiological impacts on the cells are biomechanical.

Cells anchored to their ECM exert mechanical stresses at the cell-ECM interface and also use mechanical stresses to communicate with neighboring cells (12). The mechanical stresses exerted on the ECM (tractions) are transmitted across the cells through cell-matrix junctions, such as integrins, and

Correspondence: R. L. Steward, Jr (rstewardjr@ucf.edu); V. A. S. Balachandar (vignesharavindsb@knights.ucf.edu).
Submitted 21 March 2023 / Revised 2 June 2023 / Accepted 9 June 2023

these mechanical stresses are subsequently transmitted across cell-cell junctions and exerted between cells upon their neighbors (intercellular stresses; 12). Cell-cell junctions enable fast, long-distance force communication through intercellular stresses, which balance the tractions (12). Tractions exerted on the ECM are used as a metric to characterize cell contractile forces and we measure tractions using traction force microscopy (TFM; 13–16). This method computes the tractions based on the recorded displacement field of the underlying matrix. Building upon TFM, we measure mechanical stresses generated between cells using monolayer stress microscopy (MSM). MSM recovers intercellular stresses from a monolayer of cells by treating the monolayer mathematically as a sheet of elastic, thin plates and imposing Newton's force balance and strain compatibility equations (17).

Studying the mechanical stresses mentioned earlier are critical as they have each been suggested to be important to a host of fundamental biological processes. In fact, tractions have been shown to be important in cell adhesion, spreading, migration, and ECM remodeling (14, 18–20) and is linked to various pathologies including cancer metastasis, fibrosis, and inflammation (19, 21–24). Intercellular stresses are and have been suggested to be important in tissue morphogenesis, epithelial-mesenchymal transition, wound healing, and tumor progression (25–28).

Upregulation of endothelial contractility and increase in tractions via actin stress fiber and ECM remodeling are linked to higher cellular and vascular stiffness and vascular hyperpermeability as seen in hypertension and atherogenesis (29–31). Furthermore, tractions and intercellular stresses have been linked to vascular hyperpermeability via ROCK1/2 and thrombin-mediated pathway. Such hyperpermeability induces loss of blood-brain barrier integrity and has also been linked with several neurological disorders such as multiple sclerosis, stroke, and traumatic brain injury (32, 33).

Although basement membrane typically consists of collagen IV, XV, XVIII, laminins, nidogen etc. (10), a transition to type 1 collagen was observed during embryonic vasculogenesis and in adult angiogenesis, driving outward migration (10). Furthermore, high FN accumulation was observed in atherosclerosis, leading to inflammatory signaling (11). As discussed, it is evident that changes in ECM composition have clear pathological and physiological implications, specifically the transition from native ECM composition to type 1 collagen during angiogenesis or increased FN deposition as seen in atherosclerosis (10, 11). However, the extent to which Col-I or FN composition influence the cell-derived mechanical stresses and cellular mechanical behavior in general remains unclear. To shed more light on the implications ECM can have on the cell mechanics, we measured tractions, strain energy, intercellular stresses, and morphological parameters including cell area and circularity after cells were seeded on soft hydrogels coated with the following ECM ratios: *1*) 100% Col-I, *2*) 75% Col-I-25% FN, *3*) 50% Col-I-50% FN, *4*) 25% Col-I-75% FN, and *5*) 100% FN. About 1.2 kPa hydrogels were used for the experiments to mimic the stiffness of the endothelium (~1–5 kPa) present in the tunica intima of the blood vessel (34). This study uses cutting-edge microscopy techniques to make biomechanical force measurements and investigate the topic of cell-ECM mechanotransduction. Furthermore, this paper presents as a proof of concept, illustrating the impact of the ECM on cell biomechanics.

MATERIALS AND METHODS

Cell Culture

Human umbilical vein endothelial cells (HUVECs) were cultured in Medium 200 supplemented with 1% penicillin-streptomycin (Corning) and large vessel endothelial supplement (LVES) solution. HUVECS, Medium 200, and LVES were purchased from Thermo Fisher. HUVECs from passages 12–14 were cultured in 0.1% gelatin-coated flasks at 37°C and 5% CO_2 before running all the experiments.

Polyacrylamide Gel Fabrication

The protocol for preparing polyacrylamide (PA) gels can be found in Ref. 35. In brief, glass bottom petri dishes (35 mm, Cellvis) were treated with bind silane solution for 45 min, rinsed with deionized (DI) water, and air dried. The PA solution is made by mixing ultrapure water, 40% acrylamide (Bio-Rad), 2% bis-acrylamide (Bio-Rad), and fluorescent beads (Texas red with 0.5 μm diameter, Invitrogen). The PA solution was mixed and placed in a vacuum chamber for 40 min. After this time, polymerization was initiated by adding 10% ammonia persulfate and *N*,*N*,*N*′,*N*′- tetramethylethane-1,2-diamine (TEMED) to the PA gel solution, which was subsequently added to the petri dish. Finally, hydrophobic coverslips were placed on top of the PA solution to allow complete polymerization of the PA solution to a PA gel. Our gels had a stiffness of ~1.2 kPa and height of ~100 μm (36).

Cellular Micropattern Stamp Preparation

Cellular monolayers were micropatterned to allow us to have reproducible monolayer sizes for each experiment. Micropatterning also allows us to visualize the entire monolayer and define monolayer stress-free boundary conditions, which is essential for the most precise calculation of intercellular stresses (17, 37). Polydimethylsiloxane (PDMS) was used to fabricate thin micropatterns as described previously in Refs. 35, 36, 38. In brief, a thin cross section of PDMS (Dow Corning) was prepared by mixing silicone base with a curing agent (20:1) and the mixture was then poured into a 100-mm petri dish. The PDMS mixture in the petri dish was then incubated at 70°C overnight. Thin, circular cross sections of the cured PDMS (16 mm) were fabricated using a hole puncher. Small holes (5–6 micropatterns) were made on the circular PDMS section using a biopsy punch (world precision instruments) with diameter ~2 mm each. Results presented in this paper are from a cropped, square cross section (651 × 651 μm) within the monolayer center to mitigate any micropattern boundary artifacts.

SANPAH Burning and ECM Surface Coating

The petri dish samples with PDMS micropatterns stamped on PA gels were subjected to treatment with sulfosuccinimidyl-6-(4-azido-2-nitrophenylamino) hexanoate (Sulfo-SANPAH; Proteochem) dissolved in 0.1 M HEPES buffer solution (Fisher Scientific) and exposed to UV light for at least 8 min. After the UV treatment, SANPAH was rinsed

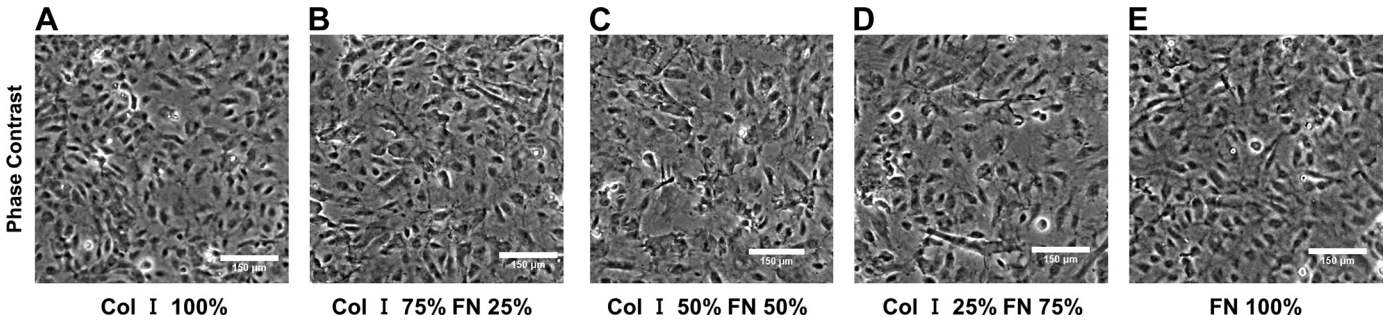

Figure 1. Cropped HUVEC monolayer phase-contrast images (within 651 × 651 μm^2) for different Col-I and FN coating concentration ratios: Col-I 100% (*A*), Col-I 75% FN 25% (*B*), Col-I 50% FN 50% (*C*), Col-I 25% FN 75% (*D*), FN 100% (*E*). Col-I, collagen I; FN, fibronectin; HUVEC, human umbilical vein endothelial cell.

off the PA gel ∼2–3 times using PBS and the PA gels were coated with ECM at a total concentration of 0.1 mg/mL at one of the following ratios and compositions: *1*) 100% Col-I (0.1 mg/mL), *2*) 75% Col-I and 25% FN, (0.075 and 0.025 mg/mL), *3*) 50% Col-I and 50% FN (0.05 and 0.05 mg/mL), *4*) 25% Col-I and 75% FN (0.025 and 0.075 mg/mL), and *5*)100% FN (0.1 mg/mL). ECM-coated gels were placed in the refrigerator overnight at 4°C and after this time excess ECM protein solution was carefully removed and HUVECs were seeded at a density of ∼50 × 10^4 cells/mL. After 60–75 min, micropatterns were carefully removed from the PA gel leaving us with circular 2-mm diameter circular patterns. Other groups have previously reported ECM remodeling to occur approximately after 2–3 days of culture (39). Therefore, to mitigate any potential contribution of ECM remodeling to our results, all experiments were run 24 h after seeding on polyacrylamide gels.

Time Lapse Microscopy

An inverted ZEISS microscope equipped with a ×5 objective and Hamamatsu camera was used to acquire bright-field images and fluorescent images at 5-min intervals for 3 h.

Traction Force Microscopy and Monolayer Stress Microscopy

Traction force microscopy (TFM) and monolayer stress microscopy (MSM) were used to calculate tractions and intercellular stresses, respectively (13, 16, 17, 35). In brief, the cell-

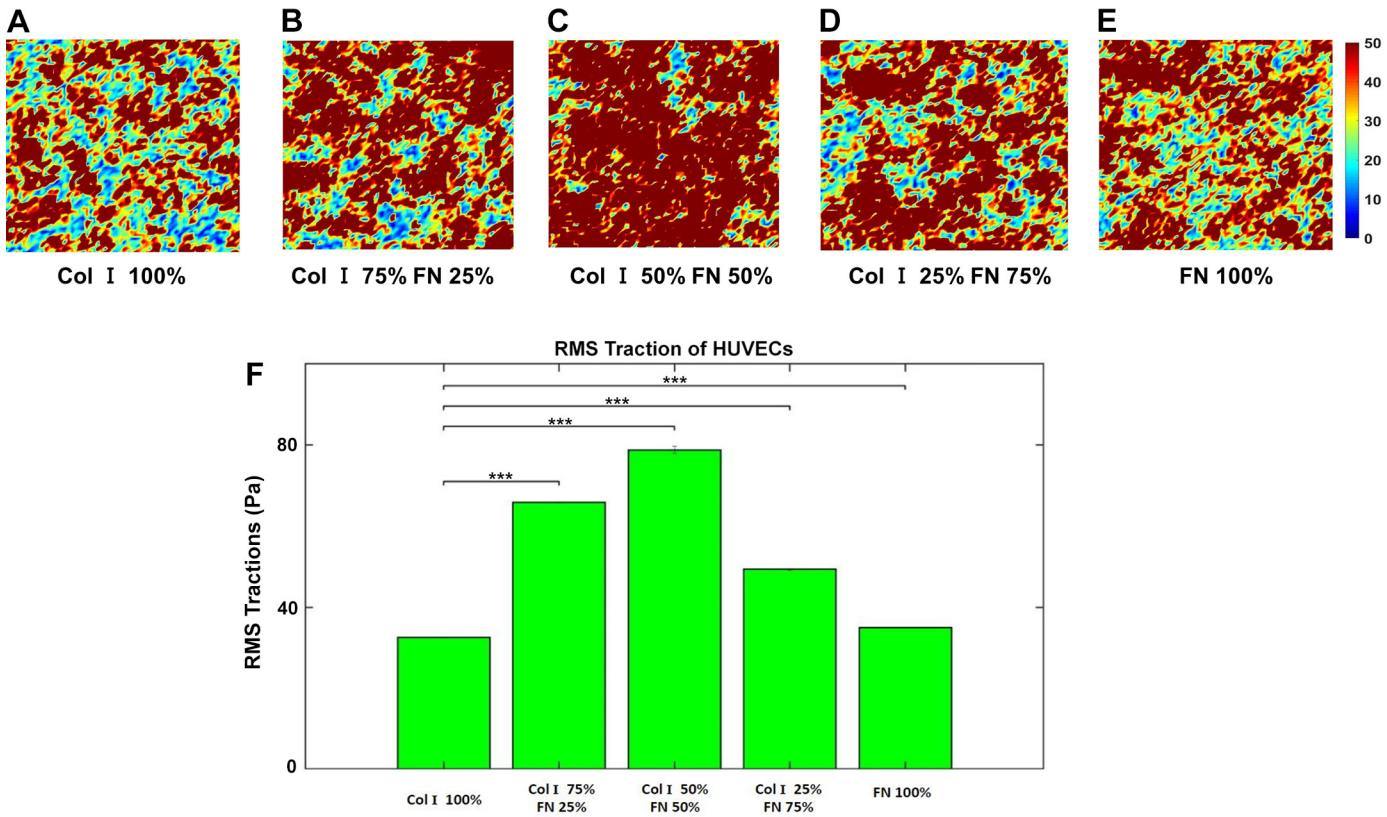

Figure 2. RMS traction (within 651 × 651 μm^2 cropped section) distributions (Pa) for different Col-I and FN coating concentration ratios: Col-I 100% (*A*), Col-I 75% FN 25% (*B*), Col-I 50% FN 50% (*C*), Col-I 25% FN 75% (*D*), FN 100% (*E*), and average RMS tractions (Pa) for different Col-I and FN coating concentrations based on averages from five samples for each ratio (*F*). *Statistical significance (***$P \leq$ 1E-3). Error bars represent standard errors. Col-I, collagen I; FN, fibronectin; HUVEC, human umbilical vein endothelial cell; RMS, root mean square.

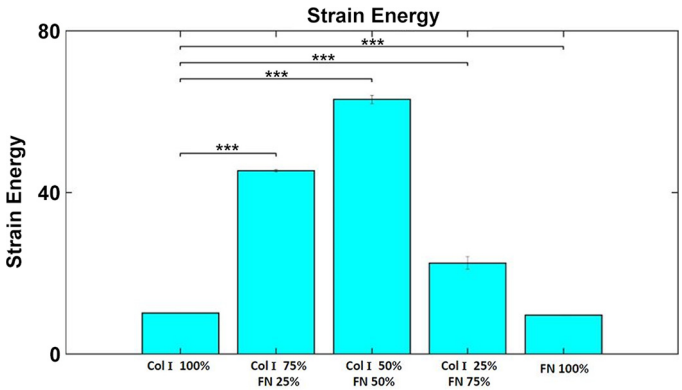

Figure 3. Average strain energies (pJ) for different Col-I and FN coating concentrations based on averages from five samples for each ratio. *Statistical significance (***$P \leq$ 1E-3). Error bars represent standard errors. Col-I, collagen I; FN, fibronectin.

induced deformations on the top surface of the gel were calculated by running a custom-written, window-based particle image velocimetry routine that computes the pixel shift of fluorescent images of the gel (cells attached) with respect to the stress-free reference image (fluorescent image taken after cell trypsinization). These displacements were then used to calculate tractions as shown by Butler et al. (16). A window size of 32 and overlap of 0.75 was used. Building upon TFM, MSM was used to calculate intercellular stresses as previously described by Trepat et al. (14). The intercellular stresses were recovered from traction force maps on the substrate by using a straightforward force balance imposed by Newton's law. The computed local two-dimensional stress tensor within the monolayer was converted into maximum principal stress (σ_{max}) and minimum principal stress (σ_{min}) along the principal plane by rotating the local coordinate system along the principal orientation. The maximum principal stress and minimum principal stress were used to calculate the average normal stress ($\sigma_{max} + \sigma_{min}$)/2 and maximum shear stress ($\sigma_{max} - \sigma_{min}$)/2. A cropped section of 651 $\times$ 651 μm was used for the analysis of tractions and intercellular stresses.

Measurement of Cell Velocity

Cellular velocity of HUVECs in the monolayer was computed using a particle image velocimetry (PIV) routine custom written in MATLAB. Cell displacements were calculated from pixel shift between phase images at two consecutive time points. The velocity map of the cells in the monolayer was calculated by averaging the change in displacements over the time interval. Cell velocity was calculated at every 5 min interval for the entire sequences of images acquired over 3 h. A cropped section of 651 $\times$ 651 μm was used for the analysis mentioned earlier.

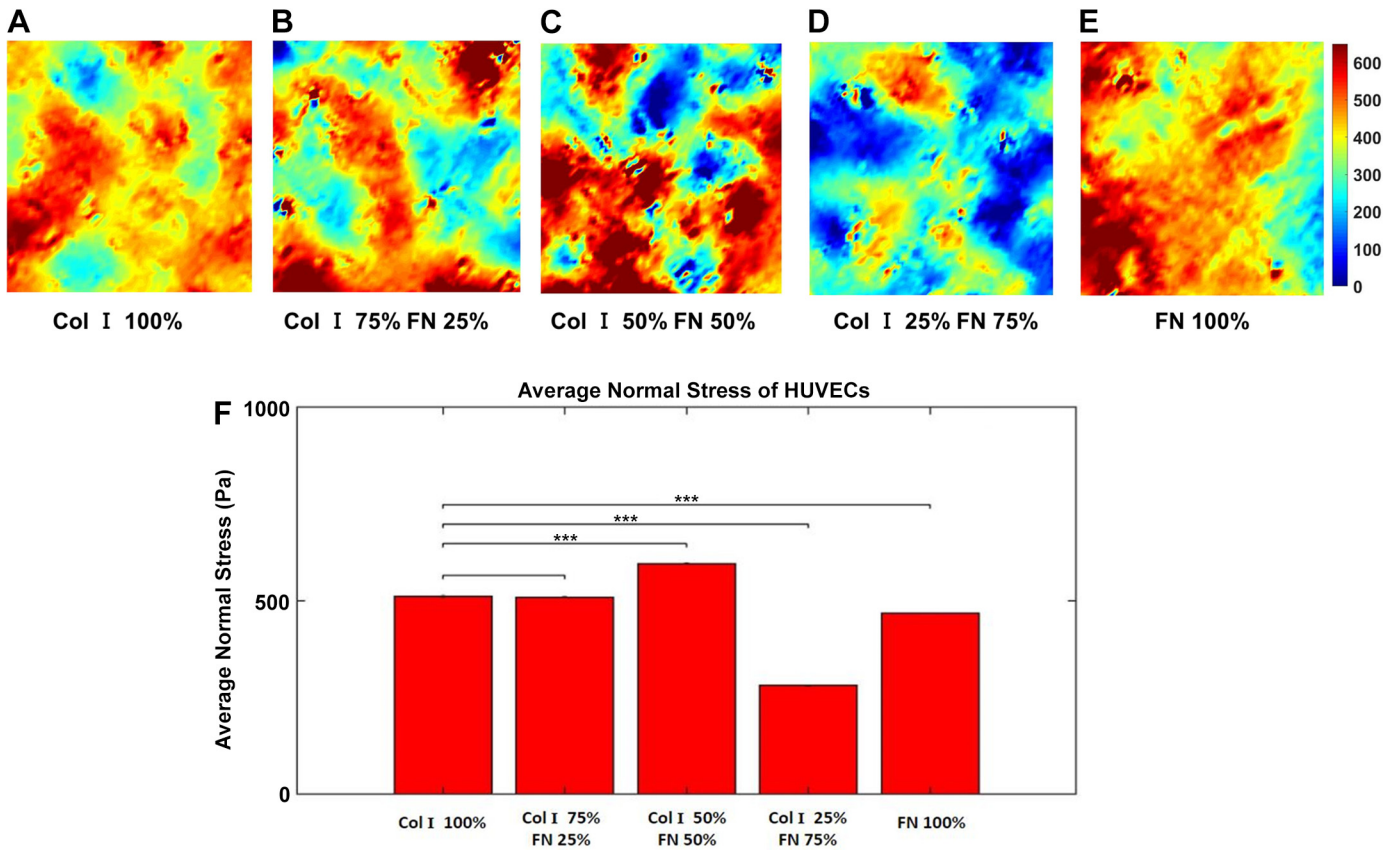

Figure 4. Average normal stress (within 651 $\times$ 651 μm^2 cropped section) distributions (Pa) for different Col-I and FN coating concentration ratios: Col-I 100% (*A*), Col-I 75% FN 25% (*B*), Col-I 50% FN 50% (*C*), Col-I 25% FN 75% (*D*), FN 100% (*E*), and average normal stress (Pa) for different Col-I and FN coating concentrations based on averages from five samples for each ratio (*F*). *Statistical significance (***$P \leq$ 1E-3; no star $P >$ 0.05). Error bars represent standard errors. Col-I, collagen I; FN, fibronectin; HUVEC, human umbilical vein endothelial cell.

Cell Area and Circularity Measurements

Cell area and cell circularity were measured using a custom feature extraction function written in MATLAB. This algorithm, which uses the image processing toolbox, allows us to calculate the properties mentioned earlier by first converting phase-contrast images to binary images, which are then segmented so each individual cell can be identified. Second, each cell is assigned a number, and finally, we extract cell area and circularity, from our binary images using MATLAB. Our algorithm calculates the cell area as the number of pixels contained in a region (sq. pixels) and converts this to μm^2 based on a pixel to micron conversion factor. The circularity, which is equal to $(4 \times \pi \times \text{area})/(\text{perimeter}^2)$ is a dimensionless number that tells us how close the cell's shape is to a circle. Circularity values range from 0 to 1 with a value of 1 representing a perfect circle, whereas values further from 1 represent a deviation from a circular shape. More information on experimental and computational methodology can be found in the Supplemental material: https://doi.org/10.6084/m9.figshare.23113370.

Statistical Analysis

The number of cells analyzed were 1,057 to 1,460 cells for each ECM coating concentration ratio. Each Col-I and FN coating ratio (75% Col-I-25% FN, 50% Col-I-50% FN, 25% Col-I-75% FN, and 100% FN) was tested for statistical significance with respect to the 100% Col-I condition using ANOVA: single-factor hypothesis test for cell area, cell orientation, and circularity respectively. The P values for significance were calculated with an α level of 0.05 (null hypothesis rejected for $P < 0.05$).

RESULTS

Tractions and Strain Energy Are Maximal at 50% Col-I- and 50% FN-Coated Substrates

Phase-contrast images of HUVECS adhered to polyacrylamide (PA) gels coated with the following Col I-FN ratios *1*) 100% Col-I, *2*) 75% Col-I and 25% FN, *3*) 50% Col-I and 50% FN, *4*) 25% Col-I and 75% FN, and *5*) 100% FN are shown in Fig. 1. The average traction distributions are shown in Fig. 2, *A–E*, and traction plot (Fig. 2*F*) revealed tractions to be highest for cells seeded on 50% Col-I- and 50% FN-coated gels with a magnitude of 78.7 ± 0.8 Pa. Tractions were the lowest for cells seeded on 100% Col-I (32.6 ± 0.05 Pa) and 100% FN (35 ± 0.06 Pa; Fig. 2*F*). The root mean square (RMS) traction was highest for 75% Col-I and 25% FN (65.8 ± 0.12 Pa) after 50% Col-I and 50% FN and above 25% Col-I and 75% FN (49.3 ± 0.2 Pa; Fig. 2*F*). The computed average strain energies followed the same trend as RMS tractions. Col-I (50%) and 50% FN had the highest strain energy (63 ± 1 pJ) followed by 75% Col-I and 25% FN (45.4 ± 0.3 pJ) and 25% Col-I and 75% FN (22.58 ± 1.6 pJ; Fig. 3).

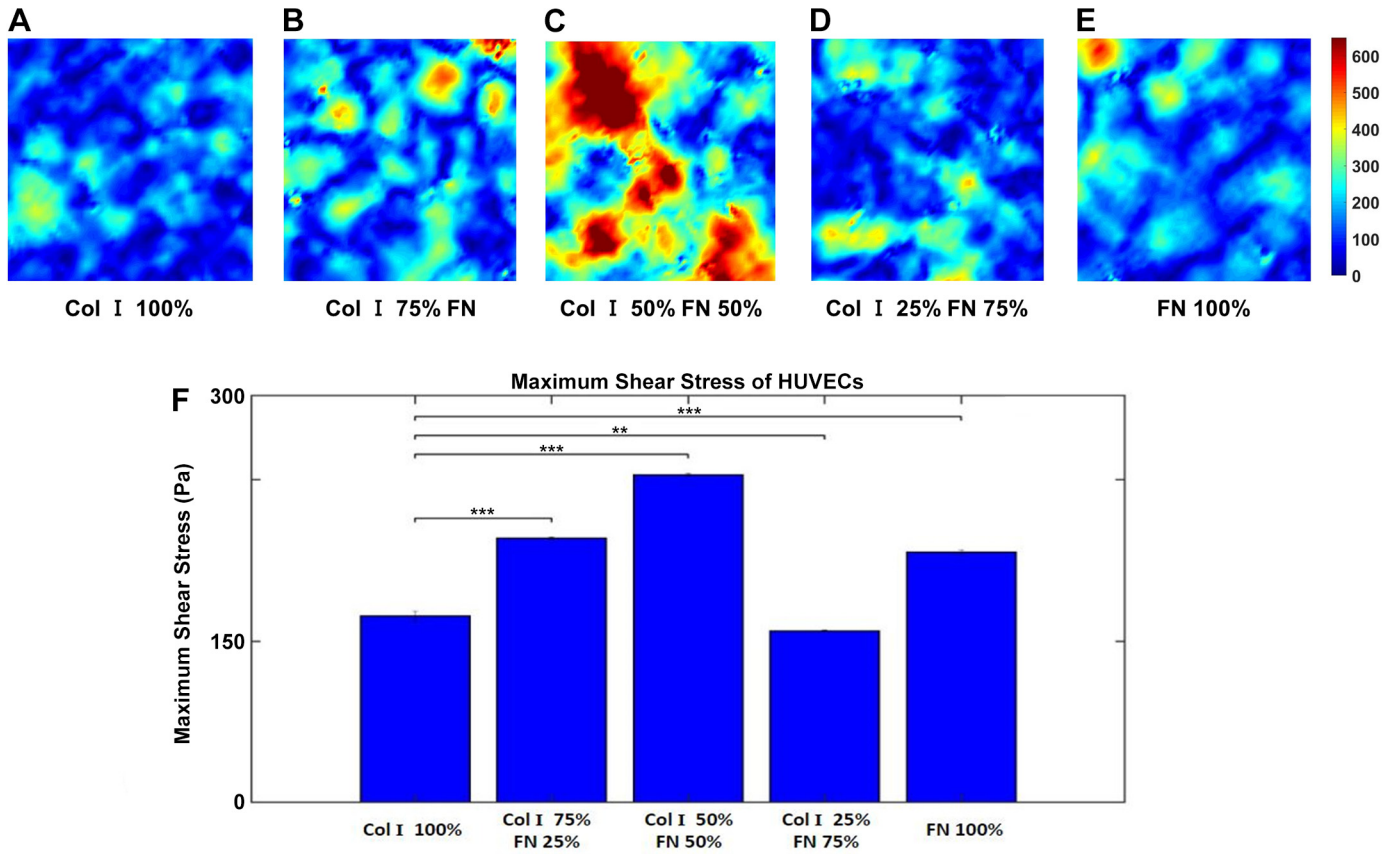

Figure 5. Maximum shear stress (within 651 × 651 μm^2 cropped section) distributions (Pa) for different Col-I and FN coating concentration ratios: Col-I 100% (*A*), Col-I 75% FN 25% (*B*), Col-I 50% FN 50% (*C*), Col-I 25% FN 75% (*D*), FN 100% (*E*), and average maximum shear stress (Pa) for different Col-I and FN coating concentrations based on averages from five samples for each ratio (*F*). *Statistical significance (**$P \leq$ 1E-2; ***$P \leq$ 1E-3). Error bars represent standard errors. Col-I, collagen I; FN, fibronectin; HUVEC, human umbilical vein endothelial cell.

FN (100%) had the least average strain energy (9.73 ± 0.075 pJ) followed closely by 100% Col-I with 10.25 ± 0.083 pJ as shown in Fig. 3. *P* values were ≤ 1E-3 for all the observed differences using one-way ANOVA test.

Intercellular Stress Response Is Maximal on 50% Col-I-50% FN

Figure 4, *A–F*, and Fig 5, *A–F*, show the average normal intercellular stress and maximum shear intercellular stress as a function of various Col-FN ratios. Both the average normal intercellular stress and maximum shear intercellular stress magnitudes were highest for 50% Col-I and 50% FN with a value of 596 ± 1.6 Pa and 304.5 ± 1.4 Pa, respectively (Fig. 4*F* and Fig. 5*F*). Similarly, average normal and maximum shear intercellular stresses were lowest for 25% Col-I and 75% FN ECM ratio with 281.5 ± 2.2 Pa and 159.7 ± 0.7 Pa, respectively. There was no statistically significant difference between 100% Col I and 75% Col-I and 25% FN with respect to average normal stress. The average normal stress was lower for 100% FN (~468.17 Pa) compared with 100% Col-I (~511.6 Pa). The maximum shear stress was slightly higher for 100% Col-I compared with 25% Col-I and 75% FN. The maximum shear stress was the second highest for 75% Col-I and 25% FN, which was slightly higher than 100% FN (Fig. 5, *A–F*). *P* values were ≤ 1E-2 for all the observed differences using one-way ANOVA test.

Cellular Velocities Are Maximal on 100% Col-I-Coated Substrates

Although tractions and strain energies were highest on 50% Col-I and 50% FN, this was not the case for cell velocities (Fig. 6, *A–F*). In fact, cell velocity was lowest for 50% Col-I and 50% FN with an average value of 0.205 ± 0.004 μm/min, but highest for 100% Col-I with an average velocity 0.305 ± 0.01 μm/min (Fig. 6*F*). The velocity for other ECM ratios was only slightly higher compared with 50% Col-I and 50% FN (from Fig. 4*F*). *P* values were ≤ 1E-3 for all the observed differences using one-way ANOVA test.

Cell Area and Cell Circularity Display Divergent Responses

Our analysis of cellular morphological response to various ECM compositions displayed opposing responses. Cell area was observed to be the highest for 50% Col-I and 50% FN (521 ± 8.3 μm^2) and the lowest for 100% Col-I (425.515 ± 4.3 μm^2) when compared with other Col I-FN ratios (Fig. 7, *A–F*). In contrast, cell circularity (Fig. 8) displayed an almost inverse behavior relative to cell spread area. Circularity is a dimensionless number that ranges from 0 to 1, with 1 representing a shape that is a

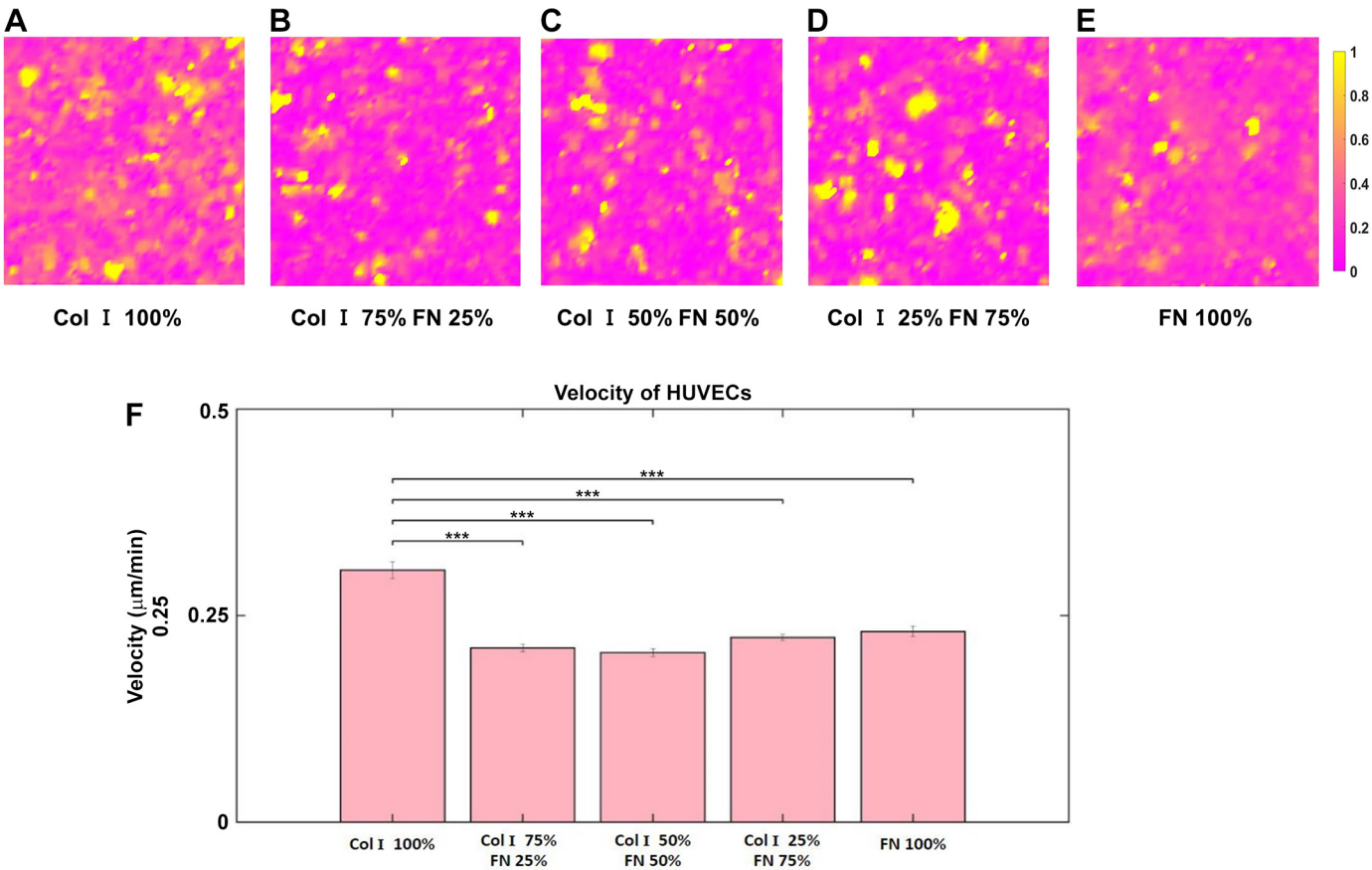

Figure 6. RMS velocity (within 651 × 651 μm^2 cropped section) distributions (μm/min) for different Col-I and FN coating concentration ratios: Col-I 100% (*A*), Col-I 75% FN 25% (*B*), Col-I 50% FN 50% (*C*), Col-I 25% FN 75% (*D*), FN 100% (*E*), and average RMS (Pa) for different Col-I and FN coating concentrations based on averages from five samples for each ratio (*F*). *Statistical significance (***$P \leq$ 1E-3). Error bars represent standard errors. Col-I, collagen I; FN, fibronectin; HUVEC, human umbilical vein endothelial cell; RMS, root mean square.

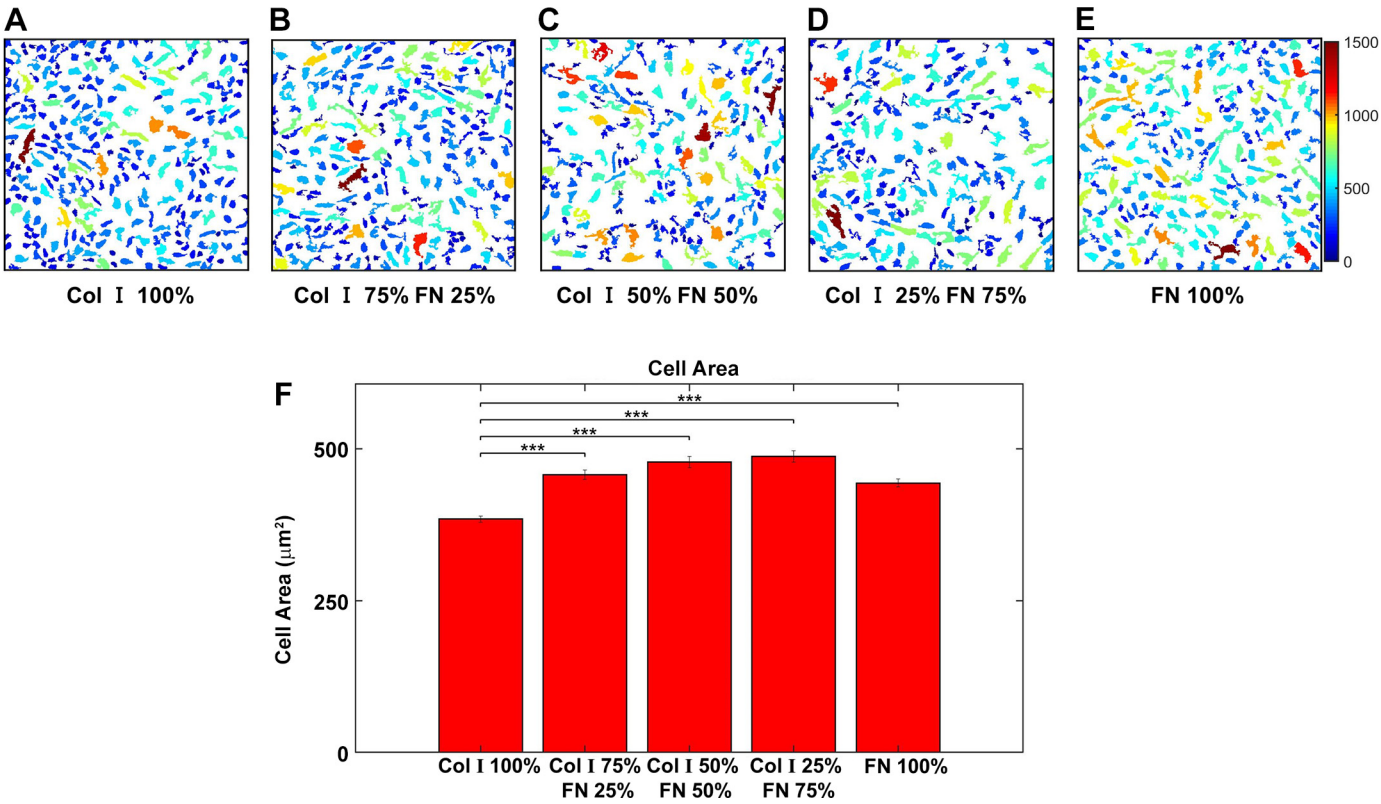

Figure 7. HUVEC area (μm^2) (within 651 × 651 μm^2 cropped section) for different Col-I and FN coating concentration ratios: Col-I 100% (*A*), Col-I 75% FN 25% (*B*), Col-I 50% FN 50% (*C*), Col-I 25% FN 75% (*D*), FN 100% (*E*), and average cell area (μm^2) for different Col-I and FN coating concentrations based on averages of 1,057 to 1,460 cells from five samples for each concentration ratio (*F*). *Statistical significance (***$P \leq$ 1E-3). Error bars represent standard errors. Col-I, collagen I; FN, fibronectin; HUVEC, human umbilical vein endothelial cell.

perfect circle. The average cell circularity was the highest for 100% Col-I (0.68 ± 0.005) and lowest for 50% Col-I and 50% FN (0.6 ± 0.006) as shown in Fig. 8*F*. Cell area and cell circularity were statistically significant when each ECM ratio group was compared with 100% Col-I case. *P* values were ≤ 1E-3 for cell area and ≤ 0.05 for cell circularity for all the observed statistical differences using one-way ANOVA test. Video of all results has been summarized in Supplemental material: https://doi.org/10.6084/m9.figshare.23115956.

DISCUSSION

The influence of the five different Col-I and FN ECM concentrations on endothelial biomechanics and morphological properties was studied. Surprisingly, 50% Col-I and 50% FN consistently revealed the highest intercellular stresses (average normal intercellular stress and maximum shear intercellular stresses) and tractions based on averages from five cropped cross sections (651 × 651 μm each from the center to avoid boundary artifacts) for each Col-I and FN ratio averaged over a period of 180 min (see Figs. 2, 3, and 4). The 50% Col-I and 50% FN also had the highest cell area, but lowest cell velocity and cell circularity. Similarly, 75% Col-I and 25% FN had the second highest average intercellular stresses and tractions, but second lowest cell velocity. However, the same expected trend was not observed with respect to average cell area and circularity for 75% Col-I and 25% FN. Also, no other consistent trends were observed for other Col-I and FN ratios.

The inverse relationship of intercellular stresses and tractions with respect to cell velocity and cell circularity observed in 50% Col-I and 50% FN could be attributed to increase in average cell area, which reduces the cell circularity as its morphology becomes more elliptical, subsequently increasing the number of cell-ECM anchor sites. Califano et al. (40) showed a positive correlation between cell spread area and traction forces, which was observed for 50% Col-I and 50% FN ratio and 100% Col-I. However, the same trend was not observed with respect to the other Col-I-FN ratios.

Ghosh et al. (41) showed that tractions were directly proportional to the substrate stiffness, but the average cell speed was inversely proportional to the substrate stiffness. Supporting this, an inverse relationship between average cell speed and tractions was observed in all the five Col-I and FN ECM ratios. However, there was no clear evidence to support the notion that tractions regulate cell speed since cell migration speed is independent of myosin II while tractions depend on it (42). It has also been shown that cell speed increases linearly for lower FN concentrations (<10 $\mu g/cm^2$), which was noticeable for increasing FN concentration in the ECM ratio (43).

High tractions and intercellular stresses observed in 50% Col-I and 50% FN and 75% Col-I and 25% ECM ratios could be explained through Col-I and FN interactions. Kubow et al. (39) showed that collagen fibers colocalize favorably with FN fibrils that are stretched. As Col-I and FN fibers stabilize, mature collagen fibers act as a protective stress shield for FN

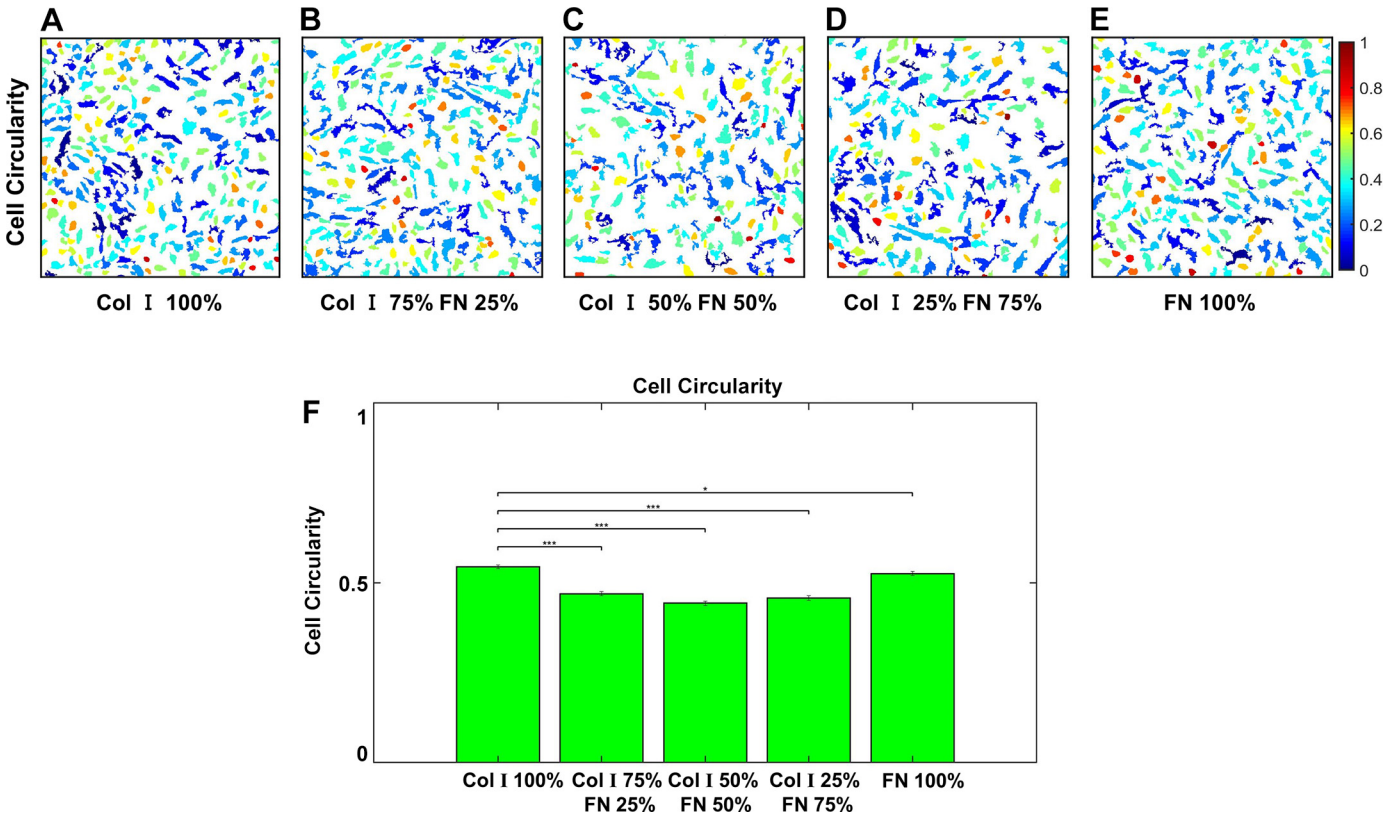

Figure 8. HUVEC circularity computed as (4 × Area × π)/(Perimeter^2) with a value of 1 for a perfect circle (within 651 × 651 μm^2 cropped section) for different Col-I and FN coating concentration ratios: Col-I 100% (*A*), Col-I 75% FN 25% (*B*), Col-I 50% FN 50% (*C*), Col-I 25% FN 75% (*D*), FN 100% (*E*), and average cell area (μm^2) for different Col-I and FN coating concentrations based on averages of 1,057 to 1,460 cells from five samples for each concentration ratio (*F*). *Statistical significance (*$P \leq 0.05$; ***$P \leq$ 1E-3). Error bars represent standard errors. Col-I, collagen I; FN, fibronectin; HUVEC, human umbilical vein endothelial cell.

fibrils (39). We propose that this one-to-one ratio of Col-I and FN might have stabilized the ECM-substrate leading to higher tractions and intercellular stresses. In addition, Lin et al. (44). showed that the cell traction forces on the substrate are proportional to the adsorption force of the FN. FN with a low adsorption force at the substrate interface might be desorbed during traction force transmission, failing to transmit the mechanical stresses to the substrate (44). The FN fibrils stabilized by collagen might have decreased the FN desorption in case of 50% Col-I and 50% FN and 75% Col-I and 25% FN ECM ratios, resulting in higher tractions and intercellular stresses relative to other ratios (44).

Conclusions

ECM plays an important role in maintaining cell physiology and abnormality in ECM deposition or composition might lead to a host of neurological and cardiovascular pathologies, and even cancer metastasis. The link between different ECM proteins and cell mechanics is currently unknown and our knowledge on endothelial mechanics with respect to different ECM proteins is very limited. We believe that our study can shed more light on the impact of two major ECM proteins (Col-I and FN) on endothelial mechanics, which are mainly linked to coronary artery diseases. Our results clearly show that substrates coated with different ratios of Col-I and FN have distinct impacts on endothelial cell biomechanical and morphological response by modifying tractions, strain energies, intercellular stresses, cell velocity, cell area, and cell circularity, under static conditions. Though true, we were unable to elucidate why tractions and intercellular stress cell mechanics were significantly higher for only 50% coating concentration ratio of Col-I and FN. In addition, although cell-derived biomechanical forces seemed to either increase or decrease depending on the Col I-FN ratios, values measured for 100% Col I and 100% FN were relatively similar in magnitude. Although investigating the underlying biomolecular mechanism driving the behavior observed here is beyond the scope of this paper, we suggest our results to potentially be a result of integrin and syndecan-ECM binding used by endothelial cells (45). Endothelial cells use α1β1 and α2β1 to bind to collagen I (46), whereas α5β1, αvβ1, αvβ3, α4β1, and αvβ5 have been reported to bind to fibronectin (45). Each of the integrin isoforms mentioned earlier have also been reported to activate common pathways beyond FAK (focal adhesion kinase), including JNK (JUN N-terminal kinase), RhoA (Ras homologous A), and Cdc42 [cell division cycle (CDC)] (45). In addition, we would also like to add that syndecans have been reported to be important to endothelial cell-ECM binding. Specifically, syndecans 2 and 4, also bind to collagen I and fibronectin, further adding to the complexity of addressing the phenomenon we report here. This suggested that pathological and physiological conditions where ECM compositions change dynamically would have the most significant impact on the

cell-derived forces and morphological parameters mentioned earlier. We believe results yielded from this study will be useful to the fields of cell mechanics, endothelial cell biology, and matrix biology. Furthermore, our results will also lead to a better understanding of the initiation and progression of various ECM-related pathologies.

DATA AVAILABILITY

The datasets used and/or analyzed during the current study are available from the corresponding author on reasonable request.

SUPPLEMENTAL DATA

Supplemental material: https://doi.org/10.6084/m9.figshare.23113370; https://doi.org/10.6084/m9.figshare.23115956.

ACKNOWLEDGMENTS

Graphical abstract created with BioRender and published with permission.

GRANTS

This work was funded by the National Heart, Lung, And Blood Institute of the National Institute of Health under award K25HL132098. This material is based on work supported by the National Science Foundation CAREER Award under Grant No. 2045750.

DISCLOSURES

No conflicts of interest, financial or otherwise, are declared by the authors.

AUTHOR CONTRIBUTIONS

V.A.S.B. and R.L.S. conceived and designed research; V.A.S.B. performed experiments; V.A.S.B. analyzed data; V.A.S.B. interpreted results of experiments; V.A.S.B. prepared figures; V.A.S.B. and R.L.S. drafted manuscript; V.A.S.B. and R.L.S. edited and revised manuscript; V.A.S.B and R.L.S. approved final version of manuscript.

REFERENCES

1. **Gao Y**, **Liu S**, **Huang J**, **Guo W**, **Chen J**, **Zhang L**, **Zhao B**, **Peng J**, **Wang A**, **Wang Y**, **Xu W**, **Lu S**, **Yuan M**, **Guo Q.** The ECM-cell interaction of cartilage extracellular matrix on chondrocytes. *Biomed Res Int* 2014: 648459, 2014. doi:10.1155/2014/648459.
2. **Wagenseil JE**, **Mecham RP.** Elastin in large artery stiffness and hypertension. *J Cardiovasc Transl Res* 5: 264–273, 2012. doi:10.1007/s12265-012-9349-8.
3. **Chiu JJ**, **Chien S.** Effects of disturbed flow on vascular endothelium: pathophysiological basis and clinical perspectives. *Physiol Rev* 91: 327–387, 2011. doi:10.1152/physrev.00047.2009.
4. **Chow MJ**, **Turcotte R**, **Lin CP**, **Zhang Y.** Arterial extracellular matrix: a mechanobiological study of the contributions and interactions of elastin and collagen. *Biophys J* 106: 2684–2692, 2014. doi:10.1016/j.bpj.2014.05.014.
5. **Sonbol HS.** Extracellular matrix remodeling in human disease. *J Microsc Ultrastruct* 6: 123–128, 2018. doi:10.4103/JMAU.JMAU_4_18.
6. **Huang Y**, **Kyriakides TR.** The role of extracellular matrix in the pathophysiology of diabetic wounds. *Matrix Biol Plus* 6–7: 100037, 2020. doi:10.1016/j.mbplus.2020.100037.
7. **Lakatta EG**, **Levy D.** Arterial and cardiac aging: major shareholders in cardiovascular disease enterprises: part I: aging arteries: a "set up" for vascular disease. *Circulation* 107: 139–146, 2003. doi:10.1161/01.cir.0000048892.83521.58.
8. **Jacob MP.** Extracellular matrix remodeling and matrix metalloproteinases in the vascular wall during aging and in pathological conditions. *Biomed Pharmacother* 57: 195–202, 2003. doi:10.1016/s0753-3322(03)00065-9.
9. **Keeley FW**, **Alatawi A.** Response of aortic elastin synthesis and accumulation to developing hypertension and the inhibitory effect of colchicine on this response. *Lab Invest* 64: 499–507, 1991.
10. **Davis GE**, **Senger DR.** Endothelial extracellular matrix: biosynthesis, remodeling, and functions during vascular morphogenesis and neovessel stabilization. *Circ Res* 97: 1093–1107, 2005. doi:10.1161/01.RES.0000191547.64391.e3.
11. **Feaver RE**, **Gelfand BD**, **Wang C**, **Schwartz MA**, **Blackman BR.** Atheroprone hemodynamics regulate fibronectin deposition to create positive feedback that sustains endothelial inflammation. *Circ Res* 106: 1703–1711, 2010. doi:10.1161/circresaha.109.216283.
12. **Patel G**, **Xu N**, **Nguyen A**, **Alvarez DF**, **Fredberg JJ**, **Stevens T**, **Tambe DT.** Mechanical signaling in a pulmonary microvascular endothelial cell monolayer. *Biochem Biophys Res Commun* 519: 337–343, 2019. doi:10.1016/j.bbrc.2019.08.169.
13. **Trepat X**, **Wasserman MR**, **Angelini TE**, **Millet E**, **Weitz DA**, **Butler JP**, **Fredberg JJ.** Physical forces during collective cell migration. *Nature Phys* 5: 426–430, 2009. doi:10.1038/nphys1269.
14. **Trepat X**, **Fredberg JJ.** Plithotaxis and emergent dynamics in collective cellular migration. *Trends Cell Biol* 21: 638–646, 2011. doi:10.1016/j.tcb.2011.06.006.
15. **Soon CF**, **Tee KS**, **Youseffi M**, **Denyer MC.** Tracking traction force changes of single cells on the liquid crystal surface. *Biosensors (Basel)* 5: 13–24, 2015. doi:10.3390/bios5010013.
16. **Butler JP**, **Tolic-Nørrelykke IM**, **Fabry B**, **Fredberg JJ.** Traction fields, moments, and strain energy that cells exert on their surroundings. *Am J Physiol Cell Physiol* 282: C595–C605, 2002. doi:10.1152/ajpcell.00270.2001.
17. **Tambe DT**, **Croutelle U**, **Trepat X**, **Park CY**, **Kim JH**, **Millet E**, **Butler JP**, **Fredberg JJ.** Monolayer stress microscopy: limitations, artifacts, and accuracy of recovered intercellular stresses. *PLoS One* 8: e55172, 2013. doi:10.1371/journal.pone.0055172.
18. **Dembo M**, **Wang YL.** Stresses at the cell-to-substrate interface during locomotion of fibroblasts. *Biophys J* 76: 2307–2316, 1999. doi:10.1016/S0006-3495(99)77386-8.
19. **Kraning-Rush CM**, **Califano JP**, **Reinhart-King CA.** Cellular traction stresses increase with increasing metastatic potential. *PLoS One* 7: e32572, 2012. doi:10.1371/journal.pone.0032572.
20. **Kraning-Rush CM**, **Carey SP**, **Califano JP**, **Smith BN**, **Reinhart-King CA.** The role of the cytoskeleton in cellular force generation in 2D and 3D environments. *Phys Biol* 8: 015009, 2011. doi:10.1088/1478-3975/8/1/015009.
21. **Indra I**, **Undyala V**, **Kandow C**, **Thirumurthi U**, **Dembo M**, **Beningo KA.** An in vitro correlation of mechanical forces and metastatic capacity. *Phys Biol* 8: 015015, 2011. doi:10.1088/1478-3975/8/1/015015.
22. **Koch TM**, **Münster S**, **Bonakdar N**, **Butler JP**, **Fabry B.** 3D traction forces in cancer cell invasion. *PLoS One* 7: e33476, 2012. doi:10.1371/journal.pone.0033476.
23. **Marinković A**, **Mih JD**, **Park JA**, **Liu F**, **Tschumperlin DJ.** Improved throughput traction microscopy reveals pivotal role for matrix stiffness in fibroblast contractility and TGF-β responsiveness. *Am J Physiol Lung Cell Mol Physiol* 303: L169–L180, 2012. doi:10.1152/ajplung.00108.2012.
24. **Jannat RA**, **Dembo M**, **Hammer DA.** Traction forces of neutrophils migrating on compliant substrates. *Biophys J* 101: 575–584, 2011. doi:10.1016/j.bpj.2011.05.040.
25. **Cetera M**, **Ramirez-San Juan GR**, **Oakes PW**, **Lewellyn L**, **Fairchild MJ**, **Tanentzapf G**, **Gardel ML**, **Horne-Badovinac S.** Epithelial rotation promotes the global alignment of contractile actin bundles during Drosophila egg chamber elongation. *Nat Commun* 5: 5511, 2014. doi:10.1038/ncomms6511.
26. **Wang S**, **Matsumoto K**, **Yamada KM.** Reconstituting Stratified epithelial branching morphogenesis by engineering cell adhesion (Preprint). *bioRxiv* 2020. doi:10.1101/2020.06.24.165795.
27. **Barriga EH**, **Franze K**, **Charras G**, **Mayor R.** Tissue stiffening coordinates morphogenesis by triggering collective cell migration in vivo. *Nature* 554: 523–527, 2018. doi:10.1038/nature25742.

28. **De Pascalis C**, **Etienne-Manneville S.** Single and collective cell migration: the mechanics of adhesions. *Mol Biol Cell* 28: 1833–1846, 2017. doi:10.1091/mbc.E17-03-0134.
29. **Maruo N**, **Morita I**, **Shirao M**, **Murota S.** IL-6 increases endothelial permeability in vitro. *Endocrinology* 131: 710–714, 1992. doi:10.1210/endo.131.2.1639018.
30. **Huynh J**, **Nishimura N**, **Rana K**, **Peloquin JM**, **Califano JP**, **Montague CR**, **King MR**, **Schaffer CB**, **Reinhart-King CA.** Age-related intimal stiffening enhances endothelial permeability and leukocyte transmigration. *Sci Transl Med* 3: 112ra122, 2011. doi:10.1126/scitranslmed.3002761.
31. **Urbano RL**, **Furia C**, **Basehore S**, **Clyne AM.** Stiff substrates increase inflammation-induced endothelial monolayer tension and permeability. *Biophys J* 113: 645–655, 2017. doi:10.1016/j.bpj.2017.06.033.
32. **Beckers CM**, **Knezevic N**, **Valent ET**, **Tauseef M**, **Krishnan R**, **Rajendran K**, **Hardin CC**, **Aman J**, **van Bezu J**, **Sweetnam P**, **van Hinsbergh VW**, **Mehta D**, **van Nieuw Amerongen GP.** ROCK2 primes the endothelium for vascular hyperpermeability responses by raising baseline junctional tension. *Vascul Pharmacol* 70: 45–54, 2015. doi:10.1016/j.vph.2015.03.017.
33. **Najjar S**, **Pahlajani S**, **De Sanctis V**, **Stern JNH**, **Najjar A**, **Chong D.** Neurovascular unit dysfunction and blood-brain barrier hyperpermeability contribute to schizophrenia neurobiology: a theoretical integration of clinical and experimental evidence. *Front Psychiatry* 8: 83, 2017. doi:10.3389/fpsyt.2017.00083.
34. **Janmey PA**, **McCulloch CA.** Cell mechanics: integrating cell responses to mechanical stimuli. *Annu Rev Biomed Eng* 9: 1–34, 2007. doi:10.1146/annurev.bioeng.9.060906.151927.
35. **Steward R Jr**, **Tambe D**, **Hardin CC**, **Krishnan R**, **Fredberg JJ.** Fluid shear, intercellular stress, and endothelial cell alignment. *Am J Physiol Cell Physiol* 308: C657–C664, 2015. doi:10.1152/ajpcell.00363.2014.
36. **Stroka KM**, **Aranda-Espinoza H.** Endothelial cell substrate stiffness influences neutrophil transmigration via myosin light chain kinase-dependent cell contraction. *Blood* 118: 1632–1640, 2011. doi:10.1182/blood-2010-11-321125.
37. **Rape AD**, **Guo WH**, **Wang YL.** The regulation of traction force in relation to cell shape and focal adhesions. *Biomaterials* 32: 2043–2051, 2011. doi:10.1016/j.biomaterials.2010.11.044.
38. **Steward RL Jr**, **Cheng CM**, **Wang DL**, **LeDuc PR.** Probing cell structure responses through a shear and stretching mechanical stimulation technique. *Cell Biochem Biophys* 56: 115–124, 2010. doi:10.1007/s12013-009-9075-2.
39. **Kubow KE**, **Vukmirovic R**, **Zhe L**, **Klotzsch E**, **Smith ML**, **Gourdon D**, **Luna S**, **Vogel V.** Mechanical forces regulate the interactions of fibronectin and collagen I in extracellular matrix. *Nat Commun* 6: 8026, 2015. doi:10.1038/ncomms9026.
40. **Califano JP**, **Reinhart-King CA.** Substrate stiffness and cell area predict cellular traction stresses in single cells and cells in contact. *Cell Mol Bioeng* 3: 68–75, 2010. doi:10.1007/s12195-010-0102-6.
41. **Ghosh K**, **Pan Z**, **Guan E**, **Ge S**, **Liu Y**, **Nakamura T**, **Ren XD**, **Rafailovich M**, **Clark RA.** Cell adaptation to a physiologically relevant ECM mimic with different viscoelastic properties. *Biomaterials* 28: 671–679, 2007. doi:10.1016/j.biomaterials.2006.09.038.
42. **Jorrisch MH**, **Shih W**, **Yamada S.** Myosin IIA deficient cells migrate efficiently despite reduced traction forces at cell periphery. *Biol Open* 2: 368–372, 2013. doi:10.1242/bio.20133707.
43. **Shiu YT**, **Li S**, **Marganski WA**, **Usami S**, **Schwartz MA**, **Wang YL**, **Dembo M**, **Chien S.** Rho mediates the shear-enhancement of endothelial cell migration and traction force generation. *Biophys J* 86: 2558–2565, 2004. doi:10.1016/S0006-3495(04)74311-8.
44. **Lin M**, **Mao S**, **Wang J**, **Xing J**, **Wang Y**, **Cai K**, **Luo Y.** Adsorption force of fibronectin controls transmission of cell traction force and subsequent stem cell fate. *Biomaterials* 162: 170–182, 2018. doi:10.1016/j.biomaterials.2018.01.036.
45. **Post A**, **Wang E**, **Cosgriff-Hernandez E.** A review of integrin-mediated endothelial cell phenotype in the design of cardiovascular devices. *Ann Biomed Eng* 47: 366–380, 2019. doi:10.1007/s10439-018-02171-3.
46. **Senger DR**, **Perruzzi CA**, **Streit M**, **Koteliansky VE**, **de Fougerolles AR**, **Detmar M.** The alpha(1)beta(1) and alpha(2)beta(1) integrins provide critical support for vascular endothelial growth factor signaling, endothelial cell migration, and tumor angiogenesis. *Am J Pathol* 160: 195–204, 2002. doi:10.1016/s0002-9440(10)64363-5.